Spatiotemporal Energy Optimization for Electrified Railways Based on a Mobile Energy Storage System

Xianlong Li
Department of Electrical Engineering
Shanghai Jiao Tong University
Shanghai, China
lixianlong@sjtu.edu.cn

Chen Shi
Department of Electrical Engineering
Shanghai Jiao Tong University
Shanghai, China
1228435629@sjtu.edu.cn

Mengyi Xu
Department of Electrical Engineering
Shanghai Jiao Tong University
Shanghai, China
xmy281309@sjtu.edu.cn

Alexis P. Zhao
Department of Energy Science & Engineering
Stanford University
CA, USA
alexzhao@stanford.edu

Da Xie
Department of Electrical Engineering
Shanghai Jiao Tong University
Shanghai, China
xieda@sjtu.edu.cn

***Abstract*-Regenerative braking is a significant source of recoverable energy in electrified railways. However, much of this energy remains underutilized due to the temporal and spatial mismatch between energy generation and traction demand. This paper proposes an optimization framework based on the Mobile Energy Storage System (MESS) for railway traction substations, integrating photovoltaic (PV) systems and MESS to achieve spatiotemporal coordination of energy utilization. A multi-timescale mixed-integer optimization model is developed, capturing minute-level variations in traction load, PV generation, and storage dynamics, while optimizing MESS routing and dwelling decisions at the hourly resolution. A case study of Shanghai's railway network is used to compare three scenarios: baseline, stationary storage system, and MESS. The results show that the MESS reduces grid energy purchases by 94% and CO_2 emissions by 90% compared to the baseline, achieving a braking-energy recovery rate of 99.2%. The proposed framework effectively enhances renewable energy utilization, reduces operational costs, and provides a novel technical solution for the low-carbon operation of electrified railways.**

Keywords—Regenerative braking energy recovery, Mobile energy storage system (MESS), Electrified railway, Spatiotemporal optimization.

I. Introduction

With the continuous expansion of railway transportation and the ongoing improvement in electrification, electrified railways have become a key component of modern transportation systems [1]. During the frequent start-stop operations of trains, traction substations face significant energy fluctuations and efficiency challenges. However, due to the widespread use of single-phase AC traction systems and constraints related to power quality, system protection, and safety isolation, much of this braking energy cannot be fed directly back into the grid and is instead dissipated through braking resistors, leading to considerable energy waste and increased thermal load on equipment [2]. This issue is particularly prominent in high-density urban railways and terminal stations, severely restricting improvements in railway system energy efficiency and carbon reduction [3].

To enhance energy utilization efficiency in traction systems, various braking energy recovery and reuse solutions have been proposed by both academia and industry. Existing research primarily focuses on several approaches. The first strategy aims to enhance the utilization of regenerative braking energy by optimizing train timetables [4]. In this approach, the departure and arrival schedules of trains are coordinated to increase the likelihood that accelerating and braking trains share the same traction power section. Through this synchronization, the braking energy produced by decelerating trains can be partially absorbed by nearby accelerating ones, reducing overall energy losses and improving system efficiency. Nevertheless, the optimization process is often constrained by factors such as operation speed, train headway, and service punctuality, which limit its flexibility and large-scale applicability in practical railway operations [3]. Second, energy storage systems (ESS), which use supercapacitors or lithium-ion batteries at traction substations to absorb energy during braking and release it during acceleration, achieve temporal energy balance [5], [6]. This method is straightforward to implement and control and has been applied in some urban rail transit systems. However, as storage devices are fixed to individual stations, this method can only regulate energy locally and cannot address the significant spatial imbalance of braking energy and load demand between different stations. Furthermore, when the storage capacity is limited, surplus energy still cannot be absorbed. The third approach is the power-sharing method, which enables regenerative braking energy (RBE) utilization by transferring surplus energy to adjacent traction sections through railway power conditioners (RPCs). Installed at traction substations or sectioning posts, RPCs interconnect power phases and facilitate energy sharing across the network [7], [8]. This method improves energy utilization efficiency, but its effectiveness still depends on train operation schedules and is sensitive to timetable variations.

In summary, existing approaches to regenerative braking energy recovery each have inherent limitations. The train timetable optimization method depends on operational scheduling and lacks flexibility for large-scale application. Stationary ESS are restricted to individual substations, while the power-sharing method, though improving energy utilization, remains sensitive to train timetables. Thus, railway traction systems still face challenges in achieving spatiotemporal coordination of regenerative energy, emphasizing the need for

979-8-3315-8138-1

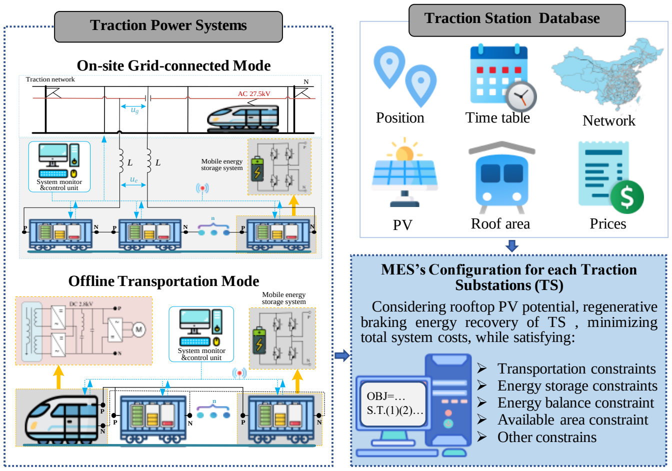

Fig.1 The proposed time-scale optimization model operation framework based on MESS

more flexible storage-based solutions.

To address these issues, this paper proposes a railway energy optimization scheme based on a Mobile Energy Storage System (MESS). The system deploys energy-storage-equipped railcars in the railway network, which, during train idle periods, connect to the traction power supply network to absorb regenerative energy and surplus PV energy. During nighttime or train downtime, the stored energy is transported to stations with higher load demand or insufficient renewable energy, enabling the dynamic transfer and reuse of energy across time and space. Compared to Stationary ESS (SESS), MESS combines the functions of both "energy absorber" and "energy carrier" and can significantly enhance system flexibility and energy utilization without changing the existing power supply structure.

II. Framework Description

Integrating PV and ESS provides a practical pathway toward carbon neutrality in railway traction substations. Installing PV panels on station rooftops and coupling them with battery systems allows for local power generation, peak-shaving, and reduced reliance on external grids. However, traditional SES can only achieve temporal balancing within individual substations and cannot mitigate spatial mismatches in regenerative energy and load distribution. As a result, surplus braking and PV energy are often wasted, hindering the low-carbon transformation of railway systems.

To address these limitations, this study develops a coordinated operation framework integrating PV and MESS, as illustrated in Fig. 1. The framework consists of three core modules:

1) Traction Power System Module: This module describes the energy interaction mechanisms of traction substations under two typical operating modes. In the On-site grid-connected mode, PV and MESS collaborate to support local power balance at the station level. In the offline transportation mode, the MESS operates during train idle periods, transferring energy across substations through railway corridors, thus redistributing energy spatially.
2) Traction-Station Database Module: This module integrates multi-dimensional data such as station locations, train schedules, rooftop areas, solar irradiation, and regional electricity prices, providing the necessary data support for system optimization.
3) MESS Configuration and Optimization Module: Using inputs such as traction load curves, PV output, and regenerative braking energy, this module develops a multi-timescale mixed-integer optimization model. The model captures the dynamic variations of storage power and PV output at the minute-level timescale, while optimizing MESS routing and dwelling strategies at the hourly timescale to achieve unified optimization of economic and energy efficiency.

This framework facilitates datasets and functional coupling between the traction power system, station database, and the MESS optimization model, providing the structural foundation and technical support for the development and computational validation of subsequent energy optimization models.

III. Multi-Timescale Optimization Framework for MESS-Driven Railway Energy Systems

To achieve low-carbon and efficient operation of traction substations, this paper proposes a coordinated optimization model integrating PV and MESS. The model aims to maximize annual overall benefits while balancing economic performance and energy utilization efficiency. It takes into account various factors, including equipment investment and maintenance, energy transmission, and mobile storage scheduling, and reflects the spatiotemporal coupling between station rooftop area, solar irradiation, train schedules, and traction load. The model optimizes storage power, PV output, and grid electricity purchases on a minute-level timescale, while optimizing the routing, dwelling status, and power distribution of MESS on an hourly timescale.

A. Objective Function

The objective of the model is to maximize the annual net benefit, which includes two main components: energy recovery benefits and costs:

$$obj = E_{en} - C_{inv} - C_{main} - C_{trans} \tag{1}$$

$$E_{en} = 365\sum_{s\in S}\sum_{t\in T}(P_{s,t}^{grid,base} - P_{s,t}^{grid,MESS})\Delta t Y_{watt} \tag{2}$$

where E_{en} represents the energy revenue generated from the traction substations based on the MESS; $s \in \mathcal{S}$ represents traction substation index; $P_{s,t}^{grid,base}$ and $P_{s,t}^{grid,MESS}$ denote the grid power purchases in the baseline (without the ESS and PV) and MESS scenarios, respectively. Y_{watt} represents the electricity price, and C_{trans} denotes the transportation cost of the MESS. C_{inv} represent the annual investment costs of the system, primarily including the costs for lithium-ion batteries, PV, and MESS, expressed as:

$$C_{inv} = C_{inv}^{pv} + C_{inv}^{bat} + C_{inv}^{car} + C_{inv}^{con} \tag{3}$$

$$C_{inv}^{pv} = \sum_{s\in S} P_s^{pv,\max} \cdot c_i^{pv} \cdot \frac{r(1+r)^{Lf^{PV}}}{(1+r)^{Lf^{PV}} - 1} \tag{4}$$

$$C_{inv}^{bat} = \sum_{m\in M} E_m^{bat,\max} \cdot c_i^{bat} \cdot \frac{r(1+r)^{Lf^{bat}}}{(1+r)^{Lf^{bat}} - 1} \tag{5}$$

$$C_{inv}^{car} = \sum_{m\in M} N_m^{car} \cdot c_i^{car} \cdot \frac{r(1+r)^{Lf^{car}}}{(1+r)^{Lf^{car}} - 1} \tag{6}$$

979-8-3315-8138-1

$$C_{inv}^{con} = \left(\sum_{s \in S} P_s^{pv,\max} + \sum_{m \in M} P_m^{bat,\max} \right) \cdot c_i^{con} \cdot \frac{r(1+r)^{Lf^{con}}}{(1+r)^{Lf^{con}} - 1} \tag{7}$$

where C_{inv}^{pv}, C_{inv}^{bat}, C_{inv}^{car} and C_{inv}^{con} represent the annual investment costs for PV, ESS, freight car, and inverters, respectively; $m \in \mathcal{M}$ denotes MESS unit index; $P_s^{pv,\max}$ and $E_m^{bat,\max}$ represent the installed capacities of PV and ESS, respectively; N_m^{car} denotes the number of freight car; c_i^{pv}, c_i^{bat}, c_i^{car} and c_i^{con} denote the unit investment cost of PV, ESS, freight car, and inverters, respectively. Lf^{PV}, Lf^{bat}, Lf^{car} and Lf^{con} represent lifetime of PV, batteries, freight car and converter, and r is discount rate.

In addition, the maintenance costs C_{main} can be expressed as

$$C_{main} = C_{main}^{pv} + C_{main}^{bat} + C_{main}^{car} + C_{main}^{con} \tag{8}$$

$$C_{main}^{pv} = \sum_{s \in S} P_s^{pv,\max} \cdot c_{main}^{pv}, C_{main}^{bat} = \sum_{m \in M} E_m^{bat,\max} \cdot c_{main}^{bat} \tag{9}$$

$$C_{main}^{car} = \sum_{m \in M} N_m^{car} \cdot c_{main}^{car} \tag{10}$$

$$C_{main}^{con} = \left(\sum_{s \in S} P_s^{pv,\max} + \sum_{m \in M} P_m^{bat,\max} \right) c_{main}^{con} \tag{11}$$

$$C_{trans} = 365 \sum_{m \in M} \sum_{t1 \in T1} M_{m,t1}^{mobile} c_{flat} \tag{12}$$

where C_{main}^{pv}, C_{main}^{bat}, C_{main}^{car} and C_{main}^{con} denotes the annual maintenance costs for PV, ESS, freight car, and inverters; c_{main}^{pv}, c_{main}^{bat}, c_{main}^{car} and c_{main}^{con} are the unit maintenance cost of PV, ESS, freight car, and inverters, respectively. C_{trans} indicates the annual transportation cost of MESS.

B. System Constraints

1) Storage System Constraints

Constraints (13)-(19) ensure the safe and physically feasible operation of the battery carried by the MESS. Constraint (13) describes the energy-state evolution of the onboard battery over each minute-level time step Δt. Constraint (14) couples the power exchange with the parking status $u_{m,s,t1}^{park}$, i.e., a MESS can release/absorb power only when it is parked and connected at station *s*; otherwise, its operating power is forced to zero. Constraint (15) imposes a state-of-charge (SOC) safety window to avoid deep cycling and preserve battery health. Constraint (16) couples the power rating and energy capacity through a C-rate limit. Constraints (17) and (18) restrict the admissible power exchange by the station hosting capability. Finally, constraint (19) converts the configured battery capacity into the required number of transport vehicles using the ceiling function, where 7.5 denotes the rated energy payload per vehicle (MWh/vehicle).

$$E_{m,t}^{bat} = E_{m,t-1}^{bat} - \sum_{s \in S} P_{m,s,t-1}^{bat} \Delta t \tag{13}$$

$$P_m^{bat,\max} u_{m,s,t1}^{parks} \le P_{m,s,t}^{bat} \le P_m^{bat,\max} u_{m,s,t1}^{park} \tag{14}$$

$$0.1 E_m^{bat,\max} \le E_{m,t}^{bat} \le 0.9 E_m^{bat,\max} \tag{15}$$

$$P_m^{bat,\max} \le 1.5 E_m^{bat,\max} \tag{16}$$

$$P_m^{bat,\max} \le P_s^{load,max} - P_s^{pos} \tag{17}$$

$$0.2 P_s^{load,max} \le P_s^{pos} \le P_s^{load,max} \tag{18}$$

$$\left\lceil E_m^{bat,con} / 7.5 \right\rceil \le N_m^{car,con} \tag{19}$$

where $E_{m,t}^{bat}$ represents the energy state of MESS *m* at time *t*; $P_{m,s,t}^{bat}$ denotes the operating power of MESS *m* at station *s*. $u_{m,s,t1}^{parks}$ indicates the parking status of MESS *m* at station *s*, and $\lceil * \rceil$ represents the ceiling function.

2) Photovoltaic System Constraints

Constraints (20)–(22) model the sizing and operational feasibility of the PV system at each station. Constraint (20) limits the maximum installable PV capacity $P_s^{pv,\max}$ by the available rooftop area and siting feasibility, ensuring that PV deployment does not exceed the physical installation potential. Constraint (21) bounds the real-time PV output $P_{s,t}^{pv}$ by the installed capacity. Constraint (22) further restricts the inter-temporal variation of PV output using a ramp-rate coefficient β, preventing unrealistically abrupt fluctuations between consecutive time steps.

$$P_s^{pv,\max} \le k^{avail} S_s^{area} \rho^{area} \tag{20}$$

$$P_{s,t}^{pv} \le P_s^{pv,\max} \tag{21}$$

$$-\beta P_s^{pv,\max} \le P_{s,t}^{pv} - P_{s,t-1}^{pv} \le \beta P_s^{pv,\max}, \tag{22}$$

where S_s^{area} denotes the available rooftop area of station *s*; ρ^{area} is the PV installable power density (kW/m^2), and k^{avail} is an availability factor accounting for practical siting constraints (e.g., shading, roof structure, and safety clearances); $P_{s,t}^{pv}$ denotes the PV output power; and β is the maximum per-step PV ramp-rate

3) Grid Power Constraints

Constraints (23)-(28) regulate the power exchange between each traction substation and the utility grid and enforce the station-level power balance. Constraint (23) and (24) bound the grid import power $P_{s,t}^{grid}$ by the admissible import capability P_s^{pos} and the traction load P_s^{load}. Constraint (25) limits an inter-temporal ramping bound on grid power, where γ is a per-step ramp coefficient reflecting operational safety and converter limitations. Constraint (26) defines the braking-resistor absorption power $P_{s,t}^{ab}$: when the net traction power $P_{s,t}^{load}$ is negative (regenerative braking dominates), the surplus energy that cannot be absorbed by local loads/storage is dissipated by the braking resistor, otherwise, the absorption is zero. Finally, (27) enforces the station-level power balance among grid PV generation, MESS, traction demand, and braking-resistor absorption.

$$P_{s,t}^{grid} \le P_s^{pos} \tag{23}$$

$$P_{s,t}^{grid} \le P_{s,t}^{load} \tag{24}$$

$$-\gamma P_s^{load,max} \le P_{s,t}^{grid} - P_{s,t-1}^{grid} \le \gamma P_s^{load,max}, \quad t > 0 \tag{25}$$

$$\begin{cases} P_{s,t}^{ab} \le -P_{s,t}^{load} & P_{s,t}^{load} < 0 \\ P_{s,t}^{ab} = 0 & P_{s,t}^{load} \ge 0 \end{cases} \tag{26}$$

$$P_{s,t}^{grid} + \sum_{m \in M} P_{m,s,t}^{bat} + P_{s,t}^{pv} = P_{s,t}^{ab} + P_{s,t}^{load} \tag{27}$$

$$M_{m,t1}^{mobile} = N_m^{car} \sum_{s \in S} u_{m,s,t1}^{mobile} \tag{28}$$

979-8-3315-8138-1

where $u^{mobile}_{m,s,t1}$ indicates the MESS *m* mobile status, which is 1 if MESS *m* is traveling during t1.

4) Dispatch Model for MESS

Considering that railways typically undergo maintenance during nighttime periods, the dispatch of MESS is scheduled exclusively during these off-peak intervals. During daytime operation, MESS functions as stationary ESS units, providing power support to traction substations. When operating in transmission mode, the transportation process of MESS is modeled using a spatial network model. Constraints (29)–(37) describe the nighttime dispatch and transportation logic of the MESS.

$$\sum_{s\in S} u^{mobile}_{m,s,t1} + \sum_{s\in S} u^{park}_{m,s,t1} = 1 \tag{29}$$

$$\begin{aligned} u^{park}_{m,s,t1+1} \ge\ & u^{park}_{m,s,t1} + 1.2(u^{mobile}_{m,s,t1} - u^{mobile}_{m,s,t1-1}) + \\ & 0.4\sum_{s\in S} u^{mobile}_{m,s,t1} - \sum_{s\in S} u^{mobile}_{m,s,t1-1} - 0.8 \end{aligned} \tag{30}$$

$$\begin{aligned} u^{park}_{m,s,t1+1} \le\ & u^{park}_{m,s,t1} + (u^{mobile}_{m,s,t1} - u^{mobile}_{m,s,t1-1}) - \\ & 0.5\sum_{s\in S} u^{mobile}_{m,s,t1} - \sum_{s\in S} u^{mobile}_{m,s,t1-1} + 0.7 \end{aligned} \tag{31}$$

$$R^{mobile}_{m,t1} M \le \sum_{s\in S} u^{mobile}_{m,s,t1} \le R^{mobile}_{m,t1} \tag{32}$$

$$R^{mobile}_{m,t1} = R^{mobile}_{m,t1-1} + S^{mobile}_{m,t1} - \sum_{s\in S} u^{mobile}_{m,s,t1-1} \tag{33}$$

$$S^{mobile}_{m,t1} \ge 0 \tag{34}$$

$$u^{direction}_{m,t1} \ge \sum_{s\in S} u^{mobile}_{m,s,t1-1} + \sum_{s\in S} u^{mobile}_{m,s,t1} - 2 + \varepsilon \tag{35}$$

$$-(1-u^{direction}_{m,t1}) \le u^{mobile}_{m,s,t1} - u^{mobile}_{m,s,t1-1} \le (1-u^{direction}_{m,t1}) \tag{36}$$

$$S^{mobile}_{m,0} = 0,\quad R^{mobile}_{m,0} = 0,\quad u^{direction}_{m,0} = 0,\quad u^{park}_{m,m,0} = 0 \tag{37}$$

Constraint (29) enforces mutually exclusive operating states, i.e., each MESS is either parked at one station or in transportation mode during each period. Constraints (30) and (31) ensure consistent state transitions between parking $u^{park}_{m,s,t1}$ and transportation $u^{mobile}_{m,s,t1}$ across consecutive periods, preventing unrealistic instantaneous relocation. Constraints (32)–(34) track the remaining transportation time and travel progression when a MESS is traveling. Specifically, (32) couples the binary mobility decision with the continuous remaining-time variable. The remaining-time variable $R^{mobile}_{m,t1}$ is activated only when the MESS is in transportation mode. Constraint (33) updates the remaining time by accounting for newly incurred travel time $S^{mobile}_{m,t1}$, and (34) enforces non-negativity of $S^{mobile}_{m,t1}$, ensuring physically feasible travel progression. Constraints (35) and (36) introduce a direction indicator $u^{direction}_{m,t1}$ to prevent oscillatory back-and-forth movements across adjacent periods; a small ε is used for strict activation in the binary-logic constraints. Finally, (37) specifies the initial states to ensure a well-defined starting point for the dispatch trajectory.

IV. Case Study

To verify the effectiveness and economic feasibility of the proposed MESS-driven traction energy optimization model, a case study is conducted using the railway network in Shanghai. Actual train timetables, station classifications, and regional solar irradiation data are incorporated to analyze energy distribution and carbon reduction under three operational scenarios.

A. Research Scenarios and Data Settings

Based on railway dispatch data and the forecasting methods proposed in [9], train timetables and traction-load curves for major stations in the Shanghai area are obtained. Typical hub stations (Shanghai Hongqiao Station and Shanghai Railway Station) and surrounding stations (Yexie, Tinglin, Anting North, Xinqiao, and Chedun) are selected to construct the traction power supply network, as shown in Fig. 2. This region is characterized by high train operation frequency, with distinct daytime traction peaks and nighttime idle periods, making it suitable for analyzing cross-period dispatch of MESS. Three operational scenarios are considered for comparison:

1. Baseline scenario: Traction substations are fully supplied by the grid without PV or ESS.
2. SESS scenario: PV systems and stationary ESS are installed at each station to achieve local energy balancing.
3. MESS scenario: On the basis of PV, a dispatchable MESS fleet is added to enable inter-station energy transfer and reuse.

Fig. 2. Railway network of Shanghai.

B. Dispatch Results and Energy Distribution Characteristics

Fig. 3 shows the dispatch schedule and SOC variations of the MESS in the Shanghai railway network. It can be observed that MESS dispatch primarily occurs during the 0–6h nighttime maintenance period, when no trains are in operation, ensuring that scheduling does not interfere with railway traffic. During the daytime, MESS operates as stationary ESS, providing voltage and power support to mitigate traction load fluctuations.

As illustrated, both Shanghai Hongqiao Station and Shanghai Station, being major terminal stations, generate large amounts of regenerative braking energy during train arrivals. However, their limited storage capacity constrains local absorption, resulting in a low energy recovery rate. In contrast, smaller surrounding stations (such as Yexie, Tinglin, and Anting North) experience higher traction demand but insufficient braking energy, as most trains pass through without stopping. Through coordinated dispatch, the MESS system transfers surplus regenerative energy from terminal stations to these smaller stations during nighttime idle periods, enabling spatial energy redistribution and improving both braking energy recovery and regional energy balance.

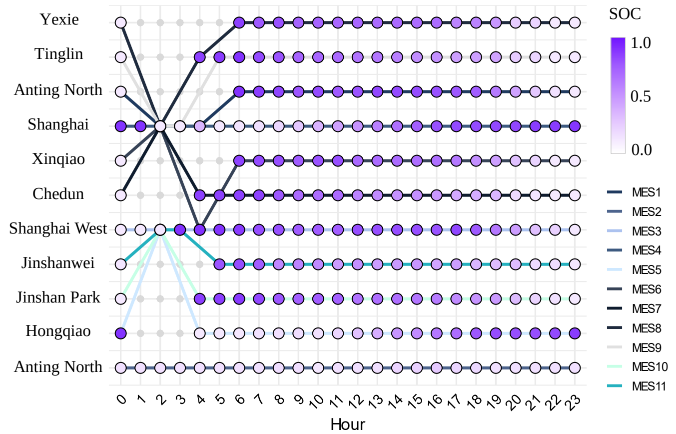

Fig. 3. Dispatch and SOC profiles of MESS in Shanghai.

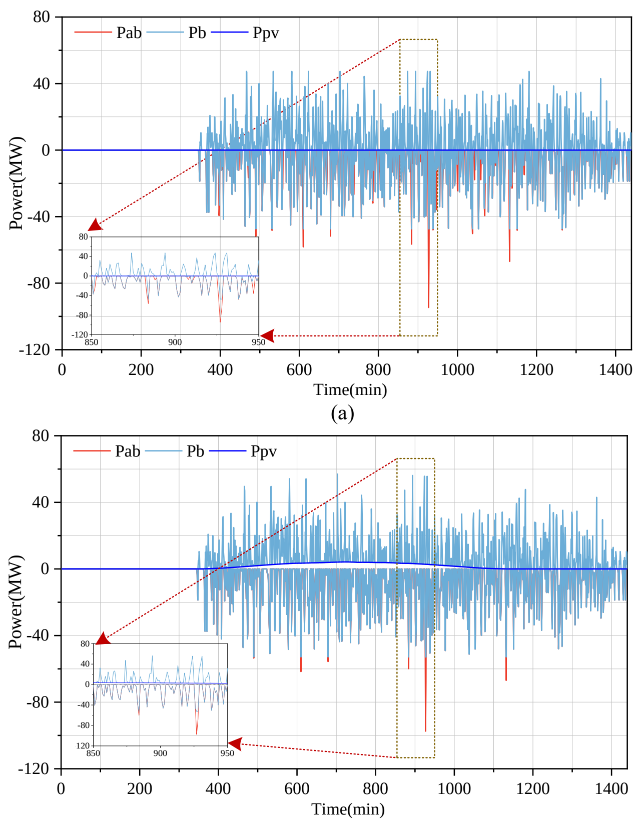

Fig. 4. Power optimization results at Shanghai Hongqiao traction substation under different scenarios: (a) Stationary ESS scenario; (b) MESS scenario.

C. Power Profiles and Comparative Analysis

Fig. 4 compares the PV output (P_{pv}), ESS (P_b), and braking resistor power (P_{ab}) at Shanghai Hongqiao Station under the stationary ESS and MES scenarios. In the stationary ESS scenario, the ESS absorbs most of the regenerative energy generated during braking, effectively mitigating grid power fluctuations. However, due to limited capacity and single-station operation, some surplus energy cannot be utilized, especially as Shanghai Hongqiao Station—being a major terminal-exhibits concentrated braking energy peaks.

In the MESS scenario, the system demonstrates stronger power regulation and energy balancing capability. Surplus energy generated during the daytime from both PV and regenerative braking is absorbed by the MESS and subsequently transported to other stations during nighttime idle hours for discharge and reuse. This enables cross-sectional energy transfer, enhances the overall recovery of regenerative energy, and further reduces the operational burden on the traction substation.

Table I. Energy and Economic Performance under Different Scenarios

Scenario	Purchased Electricity (GWh)	CO_2 Emissions (kt)	Operating Cost (10^8 USD)	BEAR
Baseline	224.01	100.98	20.41	0.00
SESS	57.33	27.75	6.13	0.88
MESS	13.41	9.61	2.75	0.99

Table II. Configuration results for the system under the MESS scenario

Station	$E_m^{bat,\max}$ (MWh)	N_m^{car} (-)	$P_s^{pv,\max}$ (MW)
Anting North	26.62	4.00	5.77
Anting West	12.64	2.00	1.33
Shanghai West	39.57	6.00	13.44
Shanghai	85.37	13.00	16.26
Shanghai Hongqiao	63.00	9.00	12.42
Xinqiao	13.21	3.00	2.75
Chedun	16.20	3.00	1.27
Yexie	12.89	2.00	1.38
Tinglin	18.39	3.00	1.28
Jinshan Park	14.00	2.00	1.42
Jinshanwei	13.04	2.00	2.55

D. Economic and Carbon Reduction Performance

To quantitatively evaluate system performance under different scenarios, statistical analyses of grid energy purchases, carbon emissions, operating costs, and braking energy recovery rates (BEAR) were conducted. The results are summarized in Table I. Here, the operating cost reported in Table I refers to the annual total cost of the traction power supply system, which includes (i) the electricity purchase cost, (ii) the annualized investment and maintenance (O&M) costs of PV, ESS, and inverters, as well as (iii) the transportation-related cost of MESS. Therefore, although the Baseline avoids investment, O&M, and transportation expenses, its annual operating cost is dominated by grid electricity purchases due to the lack of local PV supply and spatiotemporal energy shifting, leading to the highest operating cost in Table I.

Compared with the Baseline, the SESS scenario significantly improves energy efficiency: grid electricity purchases decrease from 224.01 GWh to 57.33 GWh (74% reduction), annual CO_2 emissions drop from 100.98 kt to 27.75 kt (72% reduction), and operating costs decline from 20.41×10^8 USD to 6.13×10^8 USD (70% reduction). Meanwhile, the BEAR increases from 0 to 0.88.

979-8-3315-8138-1

Building on this, the MESS scenario achieves even better overall performance: compared with the Baseline, grid energy purchases further decrease to 13.41 GWh (94% reduction), CO_2 emissions fall to 9.61 kt (90% reduction), and operating costs drop to 2.75×10^8 USD, representing an additional 55% reduction relative to the SESS scenario. The BEAR reaches 0.99, approaching full energy recovery. For completeness, the optimized sizing/configuration of the MESS fleet and PV installations under the MESS scenario is reported in Table II.

These results demonstrate that the proposed MESS can significantly reduce energy costs and carbon emissions without imposing additional burdens on the traction power network. The findings validate the proposed model's effectiveness and economic advantages in improving regenerative energy utilization, optimizing energy distribution, and supporting the low-carbon operation of railway systems.

V. Conclusion

This paper addresses the challenges of limited regenerative braking energy recovery and insufficient utilization of surplus PV energy in railway traction substations by proposing a multi-timescale energy optimization model based on MESS. The model performs fine-grained coordination of PV and ESS power at the minute-level timescale and optimizes the routing and dwelling strategies of mobile storage at the hourly timescale, thereby achieving coordinated energy management across both temporal and spatial dimensions. A case study based on the Shanghai railway network validates the effectiveness of the proposed model, and the key findings are as follows:

1) The MESS significantly improves regenerative energy recovery, achieving a maximum recovery rate of 99.2%.
2) Compared with the stationary ESS, the system reduces grid electricity purchases by approximately 77%, carbon emissions by about 65%, and overall operating costs by around 56%.
3) The proposed multi-timescale optimization framework effectively achieves coordinated optimization of energy distribution and carbon reduction while maintaining computational efficiency.

This study provides a new technical pathway for achieving low-carbon and flexible energy scheduling in railway traction power systems. Future research will further consider factors such as energy storage degradation, train operation uncertainties, and interregional grid interactions to enable broader-scale energy coordination and low-carbon dispatch.

References

[1] H. Hu, Y. Liu, Y. Li, Z. He, S. Gao, X. Zhu, and H. Tao, "Traction power systems for electrified railways: Evolution, state of the art, and future trends," *Railw. Eng. Sci.*, vol. 32, pp. 1–19, 2024.

[2] J. Chen, H. Hu, M. Wang, Y. Ge, K. Wang, Y. Huang, K. Yang, Z. He, Z. Xu, and Y. R. Li, "Power flow control-based regenerative braking energy utilization in AC electrified railways: Review and future trends," *IEEE Trans. Intell. Transp. Syst.*, vol. 25, no. 7, pp. 7089–7108, Jul. 2024.

[3] J. Chen, Y. Zhao, M. Wang, K. Wang, Y. Huang, and Z. Xu, "Power sharing and storage-based regenerative braking energy utilization for sectioning post in electrified railways," *IEEE Trans. Transp. Electrific.*, vol. 10, no. 2, pp. 2471–2483, Apr. 2024.

[4] Z. Xiao, Q. Wang, P. Sun, Z. Zhao, Y. Rao, and X. Feng, "Real-time energy-efficient driver advisory system for high-speed trains," *IEEE Trans. Transport. Electrific.*, vol. 7, no. 4, pp. 3163–3172, Dec. 2021.

[5] Y. Lu, Z. Liu, Q. Zhang, Z. Liu, H. Wang, and B. Lu, "A novel hybrid energy storage configuration framework for mountain electrified railways with long and steep slopes," *IEEE Trans. Transp. Electrific.*, vol. 11, no. 4, pp. 8756–8767, Aug. 2025.

[6] P. Luo, Q. Li, Y. Zhou, Q. Ma, Y. Zhang, and Y. Peng, "Multi-application strategy based on railway static power conditioner with energy storage system," *IEEE Trans. Intell. Transp. Syst.*, vol. 22, no. 4, pp. 2140–2152, Apr. 2021.

[7] K. Aoki, K. Kikuchi, M. Seya, and T. Kato, "Power interchange system for reuse of regenerative electric power," *Hitachi Rev.*, vol. 67, no. 7, pp. 71–75, 2018.

[8] H. J. Kaleybar, H. M. Kojabadi, M. Brenna, F. Foiadelli, and D. Zaninelli, "An intelligent strategy for regenerative braking energy harvesting in AC electrical railway substation," in *Proc. 5th IEEE Int. Conf. Models Technol. Intell. Transp. Syst. (MT-ITS)*, Naples, Italy, Jun. 2017, pp. 391–396.

[9] B. Wei, H. Hu, K. Wang, Q. Fu, and Z. He, "Research on traction load forecasting method for high-speed railway traction substation based on measured data and train timetable," *Trans. China Electrotech. Soc.*, vol. 35, no. 1, pp. 180–188, Jan. 2020.

979-8-3315-8138-1